

Mechanistic insight into 3-methylmercaptopropionate metabolism and kinetical regulation of demethylation pathway in marine dimethylsulfoniopropionate-catabolizing bacteria

Xuan Shao,¹ Hai-Yan Cao,¹ Fang Zhao,¹ Ming Peng,¹ Peng Wang,¹ Chun-Yang Li,^{1,2,3,4} Wei-Ling Shi,¹ Tian-Di Wei,¹ Zenglin Yuan,¹ Xiao-Hua Zhang,² Xiu-Lan Chen,^{1,3} Jonathan D. Todd⁵ and Yu-Zhong Zhang ^{1,2,3*}

¹State Key Laboratory of Microbial Technology, Marine Biotechnology Research Center, Shandong University, Qingdao 266237, China.

²College of Marine Life Sciences, Ocean University of China, Qingdao 266003, China.

³Laboratory for Marine Biology and Biotechnology, Qingdao National Laboratory for Marine Science and Technology, Qingdao 266237, China.

⁴Suzhou Institute of Shandong University, Suzhou, 215123, China.

⁵School of Biological Sciences, University of East Anglia, Norwich Research Park, Norwich, NR4 7TJ, UK.

Summary

The vast majority of oceanic dimethylsulfoniopropionate (DMSP) is thought to be catabolized by bacteria via the DMSP demethylation pathway. This pathway contains four enzymes termed DmdA, DmdB, DmdC and DmdD/AcuH, which together catabolize DMSP to acetylaldehyde and methanethiol as carbon and sulfur sources respectively. While molecular mechanisms for DmdA and DmdD have been proposed, little is known of the catalytic mechanisms of DmdB and DmdC, which are central to this pathway. Here, we undertake physiological, structural and biochemical analyses to elucidate the catalytic mechanisms of DmdB and DmdC. DmdB, a 3-methylmercaptopropionate (MMPA)-coenzyme A (CoA) ligase, undergoes two sequential conformational changes to catalyze the ligation of MMPA and CoA. DmdC, a MMPA-CoA dehydrogenase, catalyzes the dehydrogenation of MMPA-CoA to generate

MTA-CoA with Glu435 as the catalytic base. Sequence alignment suggests that the proposed catalytic mechanisms of DmdB and DmdC are likely widely adopted by bacteria using the DMSP demethylation pathway. Analysis of the substrate affinities of involved enzymes indicates that Roseobacters kinetically regulate the DMSP demethylation pathway to ensure DMSP functioning and catabolism in their cells. Altogether, this study sheds novel lights on the catalytic and regulative mechanisms of bacterial DMSP demethylation, leading to a better understanding of bacterial DMSP catabolism.

Introduction

The osmolyte dimethylsulfoniopropionate (DMSP) is produced in Earth's surface oceans to petagram levels annually by marine phytoplankton, macroalgae and bacteria (Ksionzek *et al.*, 2016; Reisch *et al.*, 2011a; Curson *et al.*, 2017). Indeed, DMSP production may account for as much as 10% of the total carbon fixation in some area of the ocean surface (Archer *et al.*, 2001). Environmental DMSP is utilized as an important sulfur and carbon source by taxonomically diverse bacteria, among which the Roseobacter and SAR11 clade are the most prominent members (Reisch *et al.*, 2008; Curson *et al.*, 2011). Marine bacteria catabolize DMSP via two pathways, the cleavage pathway generating the climate-active gas dimethylsulfide and the demethylation pathway (Visscher *et al.*, 1994; Reisch *et al.*, 2011a, 2011b; Li *et al.*, 2014). While ~10% of environmental DMSP is routed through the cleavage pathway, the majority of DMSP is thought to be catabolized via the demethylation pathway (Kiene *et al.*, 1999), highlighting the importance of this pathway in the marine environment.

The demethylation pathway comprises DmdA, DmdB, DmdC and DmdD enzymes (Fig. 1). DMSP is firstly demethylated by the DMSP demethylase DmdA, which catalyzes a redox-neutral methyl transfer reaction from DMSP to tetrahydrofolate (THF) to produce

Accepted 21 January, 2019. *For correspondence. E-mail zhangyz@sdu.edu.cn; Tel. +44 (0) 1603 59 2264.

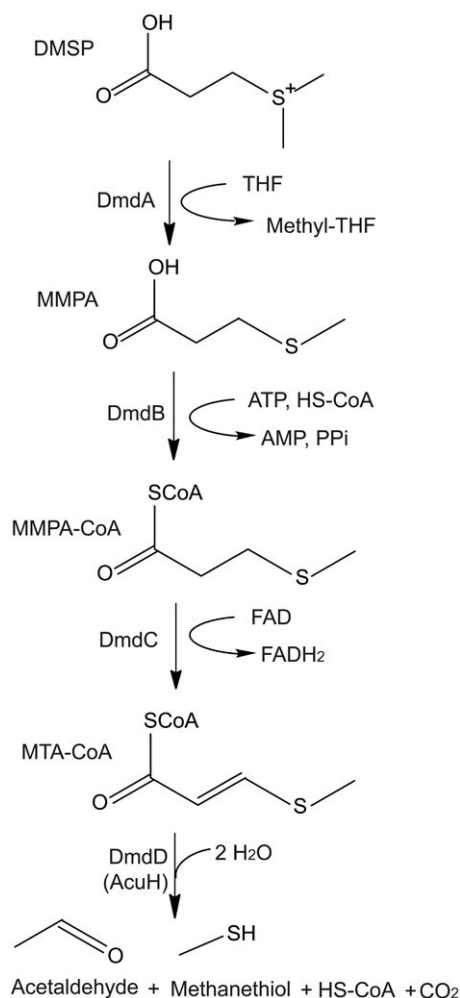


Fig. 1. Bacterial DMSP demethylation pathway. The DMSP demethylation pathway is catalyzed by the DMSP demethylase (DmdA), MMPA-CoA ligase (DmdB), MMPA-CoA dehydrogenase (DmdC) and the MTA-CoA hydratase (DmdD, AcuH).

3-methylmercaptopyruvate (MMPA) and 5-methyl-THF from DMSP (Howard *et al.*, 2006, Schuller *et al.*, 2012). Reisch *et al.* (2011b) discovered that MMPA degradation required the ligation of CoA to MMPA by the MMPA CoA ligase DmdB to generate MMPA-CoA. MMPA-CoA is then dehydrogenated by the MMPA-CoA dehydrogenase DmdC to generate methylthioacrylyl-CoA (MTA-CoA). Finally, the MTA-CoA hydratase DmdD catalyzes the hydration and hydrolysis of MTA-CoA to generate acetaldehyde and methanethiol (MeSH). Some bacteria, for example, *Ruegeria lacuscaerulensis* IT1_1157 and *Roseovarius nubinhibens* ISM, lack DmdD, but fully demethylate DMSP, utilizing a DmdD ortholog, AcuH, which functions as a MTA-CoA hydratase (Reisch *et al.*, 2011b; Bullock *et al.*, 2017). Of the Dmd enzymes, the crystal structures and the catalytic mechanisms of DmdA, DmdD and AcuH have been reported (Schuller *et al.*,

2012; Tan *et al.*, 2013; Cao *et al.*, 2017). However, the catalytic mechanisms of DmdB and DmdC are still unclear due to the lack of structural information and mechanistic studies on these enzymes.

DmdB is a class I acyl-CoA ligase family protein (cl17068). Acyl-CoA ligases adopt multiple conformations during catalysis, an open conformation (Conti *et al.*, 1996), an adenylate-forming conformation, in which the C-terminal domain of the enzyme rotates $\sim 90^\circ$ (Conti *et al.*, 1997; May *et al.*, 2002), and a thioester-forming conformation where the C-terminal domain rotates another 140° on the basis of the first rotation (Gulick *et al.*, 2003; Kochan *et al.*, 2009; Wang *et al.*, 2017). The catalytic reaction of acyl-CoA ligases is divided into two half reactions. In the first half reaction, acyl-CoA ligase undergoes the first conformational change in response to the binding of ATP from the open conformation to the adenylate-forming conformation, and the fatty acid substrate is adenylated by adenosine triphosphate (ATP) to produce an adenylate intermediate, releasing pyrophosphate (PPi) (Hisanaga *et al.*, 2004). In the second half reaction, the enzyme binds CoA to generate the thioester-forming conformation and catalyze the addition of the CoA to the adenylate intermediate to form a thioester acyl-CoA and releases an adenosine monophosphate (Kochan *et al.*, 2009). Although the transcriptional regulation and functional diversity of DmdBs have been investigated in Roseobacters, mainly *Ruegeria pomeroyi* DSS-3, and in other proteobacteria (Bullock *et al.*, 2014), the structure and catalytic mechanism of DmdB have not been studied. Thus, it is unknown whether DmdB shares a similar catalytic mechanism with similar conformational changes to those in other acyl-CoA ligases.

DmdC is an acyl-CoA dehydrogenase family protein (cl25414) (Reisch *et al.*, 2011b). Acyl-CoA dehydrogenases catalyze the initial step of fatty acid β -oxidation in the mitochondria of eukaryotic cells using flavin adenine dinucleotide (FAD) as a necessary co-factor. The reaction results in the formation of a trans double-bond between C _{α} and C _{β} of the acyl-CoA thioester substrate (Ghisla and Thorpe, 2004). Acyl-CoA dehydrogenases can use short-, medium- or long-chain fatty acid acyl-CoA as substrates, such as butyryl-CoA, C₈-CoA and C₁₁-CoA (Ghisla *et al.*, 1984; Peterson *et al.*, 1995; Ma *et al.*, 2015). Acyl-CoA dehydrogenases from different sources, such as pig liver (Kim *et al.*, 1993), plant (Ma *et al.*, 2015) and bacteria (Chowdhury *et al.*, 2014), have been characterized. Though different acyl-CoA dehydrogenases have a similar catalytic mechanism, the length of their fatty acid acyl-CoA substrate and the location of the active site differ within members of this family (Kim *et al.*, 1993). To date, three DmdC isozymes in DSS-3 have been identified and shown to have MMPA-CoA dehydrogenase activity (Reisch *et al.*, 2011b), but neither the structure

nor the catalytic mechanism of any DmdC have yet been reported.

Here, we study the DmdB and DmdC catalytic mechanisms in *R. lacuscaerulensis* ITI_1157 (ITI_1157) and *R. nubinhibens* ISM (ISM), DMSP-catabolising marine roseobacters isolated from the Blue Lagoon and the Caribbean Sea respectively (Petursdottir and Kristjansson, 1997; González *et al.*, 2003; Bullock *et al.*, 2014). The genome sequences of these model roseobacters are available (GCA_900141625.1 for ITI_1157 and GCA_000152625.1 for ISM) and both encode DmdA, B, C and D homologues. The putative *dmdB* and *dmdC* genes in these two strains were shown to up-regulated at the transcriptional level by DMSP and, when cloned, to encode functional MMPA CoA ligase and MMPA-CoA dehydrogenase enzymes. The enzymatic properties of the DmdB protein from ITI_1157 (WP_005982887.1) and the DmdC protein from ISM (WP_009812433.1) were characterized and their crystal structures were solved. Based on structural and mutational analyses of key catalytic residues, the DmdB and DmdC catalytic mechanisms were proposed. Finally, based on the analysis of the substrate affinities of DMSP demethylation pathway enzymes, we propose that the DMSP demethylation pathway is subject to kinetic regulation in DMSP-catabolizing Roseobacters. Thus, the results provide a better understanding of bacterial DMSP metabolism through the demethylation pathway.

Results and discussion

Transcriptional analysis of *dmd* genes in ITI_1157 or ISM

Roseobacters ITI_1157 and ISM are known to cleave and demethylate DMSP (González *et al.*, 2003; Curson *et al.*, 2011). The *dmdA*, *dmdB*, *dmdC* and *acuH* genes in these two strains encode products that are 29–81% identical to the functional enzymes in *R. pomeroyi* DSS-3. The transcription of *dmdA* in *R. pomeroyi* DSS-3 is known to be regulated by DMSP (Todd *et al.*, 2012). Consistent with the result in *R. pomeroyi* DSS-3, RT-qPCR analysis shows that DMSP initially (after 2 h) enhances the transcription of *dmdA* in ITI_1157 (Fig. 2A). After longer incubation time (> 4 h), the transcription of *dmdB* and *C* appears enhanced in comparison to the control sample (Fig. 2A). In comparison, the transcription of *dmdA* and *B* in ISM are only significantly enhanced after 4 h incubation with DMSP (Fig. 2B). After 6 h of incubation, *dmdA* and *B* transcription levels are almost back to the baseline level and notably *dmdC* levels increase (Fig. 2B). It is noteworthy that the ITI_1157 and ISM *dmdA*, *dmdB* and *dmdC* genes are up-regulated by DMSP in the same order as the reaction sequence in the DMSP demethylation pathway with time, perhaps suggesting that the

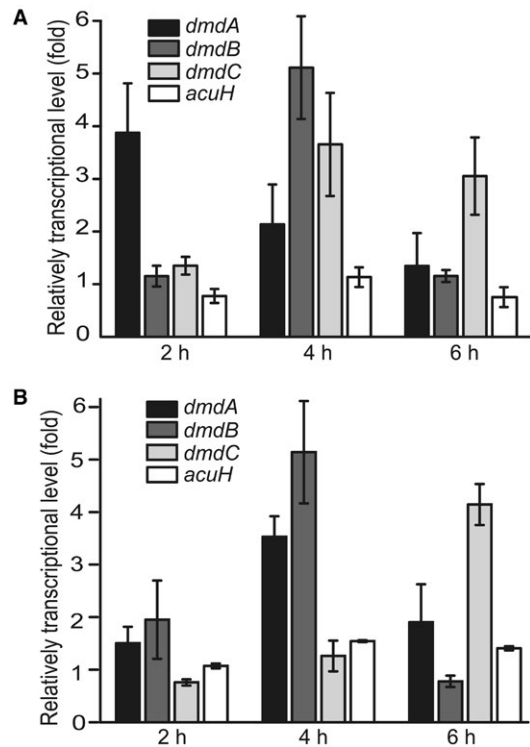


Fig. 2. Functional analysis of the genes involved in the demethylation pathway from ITI_1157 and ISM. A. RT-qPCR assay of the transcriptions of *dmdA*, *dmdB*, *dmdC* and *acuH* in ITI_1157 in response to DMSP in the medium. ITI_1157 cultured without DMSP in the medium was used as the control. The folds were calculated by comparing to the control. The *recA* gene was the house keeping gene. B. RT-qPCR assay of the transcriptions of *dmdA*, *dmdB*, *dmdC* and *acuH* in ISM in response to DMSP in the medium. ISM cultured without DMSP was used as control. The folds were calculated by comparing to the control. The *recA* gene was the house keeping gene.

product of the previous enzyme is the inducer, which needs further investigation. The transcription of *acuH* is not enhanced in response to DMSP in either ITI_1157 or ISM, consistent with its surrogate role of *dmdD* to catalyze MTA-CoA in this demethylation pathway (Reisch *et al.*, 2011b; Bullock *et al.*, 2017).

The ITI_1157 or ISM DmdABC and AcuH enzymes are functional

The *dmdABC* and *acuH* genes were cloned, over-expressed in *Escherichia coli*, purified and assayed for the enzymatic activities of their respective DMSP demethylase (DmdA), MMPA-CoA ligase (DmdB), MMPA-CoA dehydrogenase (DmdC), and the MTA-CoA hydratase (DmdD, AcuH). In each case the recombinant enzymes showed the expected activity (Fig. S1), indicating that these putative genes likely function in ITI_1157 and ISM as they do in *R. pomeroyi* DMSP demethylation pathway

(Reisch *et al.*, 2008; 2011b). Since the catalytic mechanisms of DmdA and AcuH have been described (Reisch *et al.*, 2008; Schuller *et al.*, 2012; Tan *et al.*, 2013; Cao *et al.*, 2017), the following work is focused on the catalytic mechanisms of DmdB and DmdC to reveal the molecular mechanism for MMPA metabolism in DMSP-catabolizing Roseobacters.

Characterization and overall structure analysis of DmdB and DmdC

The recombinant DmdBs and DmdCs from both ITI_1157 and ISM were subjected to crystallization. Because we failed to obtain the crystal of ISM DmdB and ITI_1157 DmdC, we focused on the characterization and structure analysis of ITI_1157 DmdB (DmdB hereafter) and ISM DmdC (DmdC hereafter).

The optimal pH and temperature for the MMPA CoA-ligase activity of purified DmdB were 8.0–9.0 (Fig. 3A) and 40°C (Fig. 3B) respectively. The crystal structure of DmdB was determined in complex with adenosine diphosphate (ADP) (DmdB/ADP) to 2.2 Å resolution (Table 1). It was shown that ADP acts as a competitive inhibitor for ATP because the MMPA CoA-ligase activity of DmdB was inhibited by ADP (Fig. S2) and the K_m value of DmdB to ATP was significantly increased when ADP was present

(Table 3). This is known to be the case in kinases or ATP-dependent H^+ transport (Roche and Reed, 1974; Pratt and Roche, 1979; Hilgenberg, 1985), but has not been reported in any other CoA-ligase. Structural data shows DmdB to be a homodimer in an asymmetric unit. Gel filtration analysis also indicated that DmdB is a dimer in solution (Fig. 4A), further supporting that DmdB functions as a dimer in the catalysis of MMPA CoA ligation. The topological structure of DmdB is similar to other acyl- or aryl-CoA synthetases (Hisanaga *et al.*, 2004). The two monomers (chains A and B) of DmdB adopt different structures in the crystals. Chain A that contains no substrate adopts the open conformation, and chain B that contains an ADP molecule adopts the adenylate-forming conformation (Fig. 4B). Structural analysis showed that DmdB chain A does not contain any substrate and is in the open conformation, while chain B contains an ADP molecule and is in the adenylate-forming conformation (Fig. 4B). Structural analysis of DmdB described below is based on the structure of chain B unless otherwise noted. Each monomer of DmdB consists of a large N-terminal domain (Met1 to Arg432, the N-domain) and a small C-terminal domain (Ser433 to Gly539, the C-domain). The active center is located at the interface between the two domains (Fig. 4C). The N-domain consists of three β -sheets (sheets 1, 2 and 3) and six helices that are sandwiched between sheet 1 and

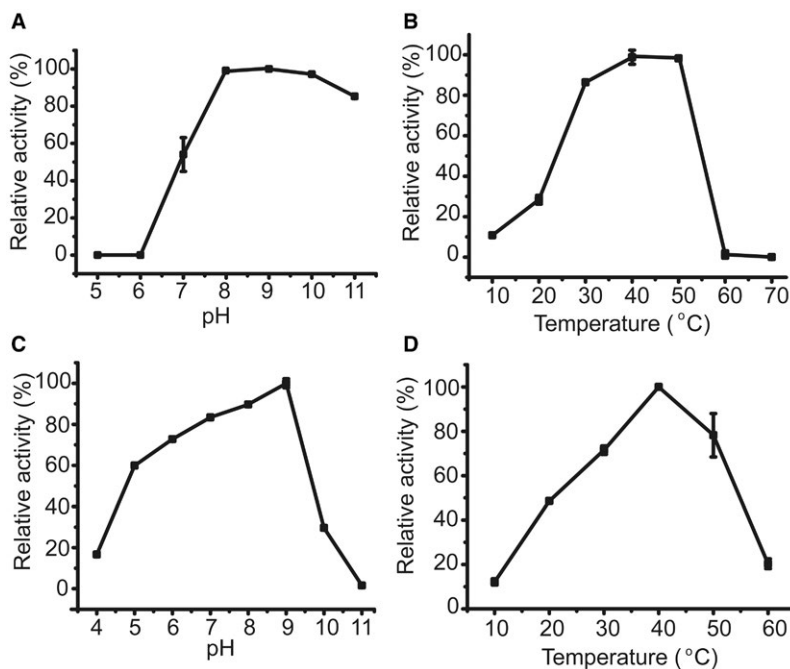


Fig. 3. Characterization of DmdB from ITI-1157 and DmdC from ISM. A. Effect of pH on the activity of DmdB. The highest activity of DmdB at pH 8.0 is taken as 100%. B. Effect of temperature on the activity of DmdB. The highest activity of DmdB at 40°C is taken as 100%. C. Effect of pH on the activity of DmdC. The highest activity of DmdC at pH 9.0 is taken as 100%. D. Effect of temperature on the activity of DmdC. The highest activity of DmdC at 40°C is taken as 100%.

Table 1. Diffraction data and refinement statistics of apo-DmdC, DmdB in complex with ADP, and Lys523Ala in complex with AMP and MMPA.

Parameters	DmdB/ADP	Lys523Ala/AMP/MMPA	apo-DmdC
Diffraction data			
Space group	P 1 21 1	P 1 21 1	P 21 21 21
Unit cell			
a, b, c (Å)	63.4 121.2 73.5	65.5 122.6 74.3	81.0 103.4 125.9
α, β, γ (°)	90.0 93.7 90.0	90.0 93.1 90.0	90.0 90.0 90.0
Resolution range (Å)	46.5–2.2 (2.3–2.2)	26.2–2.1 (2.2–2.1)	40.0–2.3 (2.4–2.3)
Redundancy	3.3 (3.4)	6.4 (6.8)	6.5 (6.6)
Completeness (%)	99.6 (99.7)	98.9 (100)	99.4 (99.3)
Rmerge [†]	0.1 (0.3)	0.1 (0.4)	0.1 (0.5)
I/sigma(I)	18.4 (5.1)	33.1 (6.0)	19.1 (3.9)
Refinement statistics			
R factor (%)	0.18	0.19	0.18
Free R factor (%)	0.22	0.22	0.22
Rmsd from ideal geometry			
Bond lengths (Å)	0.008	0.008	0.009
Bond angles (°)	1.0	1.0	0.9
Ramachandran Plot (%) [*]			
Favored	96.0	97.0	97.0
Allowed	4.0	3.2	2.6
Average B factors (Å ²)	36.4	40.9	37.5
Protein	36.3	40.7	37.4
Ligands	33.4	48.3	42.3
Solvent	38.8	43.8	38.6

Note: Numbers in parentheses refer to data in the highest-resolution shell.

[†]Rmerge = $\sum_{hkl} \sum_i |I(hkl)_i - \langle I(hkl) \rangle| / \sum_{hkl} \sum_i \langle I(hkl) \rangle$.

^{*}The Ramachandran Plot was calculated by PROCHECK program in CCP4i program package.

sheet 2 (Fig. 4C). The C-domain forms a three-stranded β -sheet (sheet 4) with three helices on its face (Fig. 4C).

Purified DmdC displayed an optimal pH of 9.0 (Fig. 3C) and an optimal temperature of 40°C (Fig. 3D). The crystal structure of apo-DmdC was determined to 2.3 Å resolution (Table 1). Both structural and gel filtration analyses showed DmdC to form a dimer in solution (Fig. 4D and 4E). The DmdC dimer is assembled through a large interface (Fig. 4E). Each DmdC monomer consists of four domains: an N-terminal α -helical domain (α -domain 1, residues 1–64 and 73–155), a ten-stranded β sheet domain (residues 65–72 and 156–280), a central α -helical domain (α -domain 2, residues 281–452) and a C-terminal α -helical domain (α -domain 3, residues 453–593) (Fig. 4F).

The catalytic mechanism of DmdB for the ligation of MMPA and CoA

To obtain the structure of DmdB in complex with substrates, several mutants were constructed according to the structure of DmdB/ADP complex, and an inactive mutant Lys523Ala was obtained. We attempted to

obtain the crystal structure of the mutant Lys523Ala in complex with ATP and MMPA, but could only determine the structure of Lys523Ala in complex with AMP and MMPA (Lys523Ala/AMP/MMPA) to 2.1 Å (Table 1). In this structure, the conformation of two chains of this complex is similar to those of the DmdB/ADP complex with a root-mean-square deviation (rmsd) of 0.3 Å. Chain A without any substrate is in the open conformation and chain B binding MMPA and AMP is in the adenylate-forming conformation. The C-domain of chain A is positioned far away from the active center (Fig. 5A), whereas the C-domain of chain B rotates ~64° from the open conformation to approach the active center (Fig. 5A). Structural alignment between chain B of complex DmdB/ADP and complex Lys523Ala/AMP/MMPA shows that Lys523 forms a hydrogen bond with MMPA to assist the catalytic localisation of MMPA (Fig. 5B). The side chain of Lys523 interacts with the phosphate moieties of ADP to help localize the phosphate moieties of ADP close to the MMPA substrate and to increase the acidity and the electrophilicity of the phosphorus (Fig. 5B), which support the finding above that ADP can function as a competitive inhibitor of ATP. These data,

together with the mutational analysis provide evidence for Lys523 playing an important role in catalysis. The replacement of Lys523 by alanine and glutamic acid both dramatically decreased the enzymatic activity of DmdB (Table 2). Circular dichroism (CD) spectroscopy analysis of wild type DmdB and its mutants showed that the secondary structures of the mutants exhibit no deviation from that of wild type DmdB (Fig. S3A), indicating that the decrease in the enzymatic activities of the mutants resulted from residue replacement rather than structural changes.

In the active center of Lys523Ala/AMP/MMPA complex, the carboxyl oxygen of MMPA and the α -phosphate of AMP form an interaction, suggesting the formation of the intermediate MMPA-AMP (Fig. 5C). Structural predictions suggest residues His231, Trp235, Gly302 and Pro333 form hydrogen bonds with MMPA (Fig. 5C). Site-directed mutations of these four residues reduced the activity of DmdB and increased its K_m value to MMPA (Tables 2 and 3), supporting the hypothesis that residues His231, Trp235, Gly302 and Pro333 in DmdB are important for MMPA binding. Residues His231, Gly303, Trp326 and Arg432 are predicted to form hydrogen bonds with AMP (Fig. 5C). Site-directed mutations of Gly303 to Pro and Trp326 to Ala almost completely abolished the activity of DmdB, but did not affect its K_m value (Tables 2 and 3), suggesting that these two residues are involved in substrate catalysis rather than binding. Site-directed mutations of His231 and Arg432 to Ala reduced the activity of DmdB and both increased its K_m value to ATP (Tables 2 and 3), indicating

that His231 and Arg432 are likely involved in ATP binding. In addition, structural alignment between chain A and chain B shows that residue Trp235 may serve as a gate for MMPA entry into the active center (Fig. 5D). In the absence of ligand, the indole ring of Trp235 extends into the active center that blocks the entry of fatty acid; in the presence of ligand, the indole ring of Trp235 swings and the entrance of the fatty acid-binding tunnel is open (Fig. 5D), just like the function of the residue Trp234 in tLFC-FACS, which is the long chain fatty acyl-CoA synthetase from *Thermus thermophilus* HB8 (Hisanaga et al., 2004).

During catalysis, acyl-CoA ligases usually go through a conformational change from the adenylate-forming conformation to the thioester-forming conformation, in which the C-domain rotates approximately 140° (Gulick et al., 2003; Hisanaga et al., 2004; And and Tong, 2004; Reger et al., 2007; Kochan et al., 2009; Wang et al., 2017). The structure of the 4-coumarate:CoA ligase (PDB code: 5BSR) is in the thioester-forming conformation (Li and Nair, 2015). To study the thioester-forming conformation of DmdB, we rotated the C-domain of DmdB according to the structure of the 4-coumarate:CoA ligase (Fig. 5E). In the modeled thioester-forming conformation of DmdB, some residues of DmdB were predicted to be in close proximity to CoA and the following mutant variants were constructed, including His231Ala, Lys434Ala, Asp435Ala, Lys438Ala, Gly440Pro, Gly441Pro, Glu442Ala, Trp434Ala, Glu474Ala and Lys526Ala. Mutations of His231, Lys434, Asp435 and Lys526 to Ala partly decreased the activity of DmdB (Table 2), but did not affect its K_m value to CoA (Tables 2 and 3), suggesting these residues are involved in catalysis. Mutations of Lys438, Glu442, Trp443, Glu474 to Ala and Gly440 and Gly441 to Pro not only decreased the activity of DmdB, but also greatly increased its K_m value to CoA (Tables 2 and 3), suggesting that these residues are involved in CoA binding.

Our mutational and structural analysis and the previously reported structures of acyl-CoA ligases (Li and Nair, 2015, Wang et al., 2017) strongly support the hypothesis that DmdB undergoes two conformational changes during catalysis, a transition from an open-form to the adenylate-form, followed by a transition to the thioester-forming conformation that ultimately catalyses the formation of MMPA-CoA via the following mechanism. Firstly, the binding of an ATP molecule causes a 64° rotation of the DmdB C-domain, leading to the first conformational change of DmdB from the open conformation to the adenylate-forming conformation. Then the substrate MMPA enters the active center and is stabilized by residues His231, Trp235 and Gly302. In the active center, MMPA serves as the nucleophilic base to attack the P_α of ATP in the nucleophilic reaction, which weakens the P_α -O bond of ATP (Fig. 7A). Then the formation of the P_α -O bond between the α -phosphate and the carboxyl oxygen of MMPA leads

Table 2. Enzymatic activities of the mutants of DmdB.^a

Enzyme	Relative activity (%)
Wild type	100
His231Ala	74.2 ± 1.4
Trp235Ala	0.5 ± 0.1
Gly302Pro	0.6 ± 0.01
Gly303Pro	0.3 ± 0.03
Trp326Ala	7.7 ± 0.7
Pro333Ala	69.5 ± 4.2
Arg432Ala	4.3 ± 0.7
Lys434Ala	36.6 ± 3.6
Asp435Ala	76.0 ± 2.7
Lys438Ala	5.6 ± 0.05
Gly440Pro	3.6 ± 0.5
Gly441Pro	2.7 ± 0.5
Glu442Ala	27.9 ± 1.1
Trp443Ala	60.9 ± 2.7
Glu474Ala	33.7 ± 0.7
Lys523Ala	1.6 ± 0.07
Lys523Glu	1.4 ± 0.2
Lys523Arg	57.2 ± 0.2
Lys526Ala	48.0 ± 2.3

^aRelative activity values expressed as a percentage of the specific activity of the wild type DmdB (100%). The standard errors are from three independent experiments. The specific activity in unit mg^{-1} of protein (\pm SE) defined as 100% was 567.4 ± 9.6 ($\mu\text{mol min}^{-1} \text{mg}^{-1}$).

Table 3. K_m values of wild type DmdB and its mutants to different substrates.

Enzyme	K_m (mM)
	To MMPA
Wild type	0.2 ± 0.02
His231Ala	4.8 ± 0.3
Trp235Ala	53.3 ± 2.4
Gly302Pro	58.0 ± 3.0
Pro333Ala	42.2 ± 2.9
	To ATP
Wild type	0.8 ± 0.05
ADP inhibitor	5.0 ± 0.2
His231Ala	3.2 ± 0.2
Gly303Pro	0.8 ± 0.1
Trp326Ala	1.1 ± 0.1
Arg432Ala	7.1 ± 0.8
	To CoA
Wild type	0.4 ± 0.01
His231Ala	0.4 ± 0.1
Lys434Ala	0.7 ± 0.1
Asp435Ala	1.7 ± 0.1
Lys438Ala	5.3 ± 0.5
Gly440Pro	10.7 ± 1.3
Gly441Pro	3.3 ± 0.2
Glu442Ala	6.0 ± 0.4
Trp443Ala	3.2 ± 0.3
Glu474Ala	5.1 ± 0.3
Lys526Ala	0.6 ± 0.04

^aThe K_m values were determined by nonlinear analysis based on the initial rates of the reactions performed at pH 8.0 and 40°C. The standard errors are from three independent experiments.

to the breaking of the P_α-O bond between the α-phosphate and the β-phosphate, forming the intermediate MMPA-AMP (Fig. 7A). Subsequently, the second conformational change happens with the C-domain rotating 140° and DmdB forming the thioester-forming conformation. In the thioester-forming conformation, CoA is stabilized by residues Asp435, Lys438, Gly440, Gly441, Glu442, Trp443 and Glu474. The sulphhydryl sulphur of CoA likely attacks the carbonyl carbon of MMPA-AMP, which weakens the C-O bond. The formation of the C-S bond between MMPA and CoA leads to the breaking of the C-O bond between MMPA and AMP, and the breaking of S-H bond of CoA. Finally, AMP is replaced by CoA and the final product MMPA-CoA is formed (Fig. 7B). After the reaction, AMP and MMPA-CoA are released from the active center, and DmdB returns to the open conformation.

To analyze the universality of the catalytic mechanism of DmdB to catalyze MMPA in marine bacteria, we performed sequence alignment of bacterial DmdBs. The result showed that residue Lys523 and most of the residues involved in the binding of MMPA, ATP and CoA are highly conserved in DmdBs from marine (including many roseobacters and the model SAR11 *Pelagibacter ubique*) and nonmarine bacteria (Fig. S4). This indicates that the proposed catalytic cycle of DmdB to oxidize MMPA into MMPA-CoA is likely adopted by most, if not all, bacterial DmdBs.

The catalytic mechanism of DmdC for MMPA-CoA redox reaction

To study the catalytic mechanism of DmdC, a molecular docking simulation of DmdC binding FAD was performed based on the structure of apo-DmdC (Fig. 6A). The FAD-binding site is contained within the extensive interface between the two monomers of DmdC. The isoalloxazine ring of FAD is buried within the binding pocket of one monomer and its other portion extends outside (Fig. 6A). The FAD molecule is stabilized by forming hydrogen bonds with residues Met161, Thr170, Phe195, Ser197 and Tyr434 (Fig. 6A). Site-directed mutations of Thr170, Ser197 and Tyr434 to Ala significantly decreased the activity of DmdC and increased its K_m value to FAD (Tables 4 and 5), indicating that these residues are involved in FAD binding. Site-directed mutation of Met161 to Ala also reduced the activity of DmdC, but did not affect its K_m value (Tables 4 and 5), and mutation of Phe195 to Ala almost completely abolished the activity of DmdC (Table 4), suggesting that these two residues are involved in substrate catalysis rather than binding. In addition, CD spectroscopy analysis showed that the secondary structures of the mutants exhibit no deviation from that of wild type DmdC (Fig. S3B), indicating that the decrease in the enzymatic activities of the mutants resulted from residue replacement rather than structural changes.

As we failed to obtain the structure of DmdC in complex with MMPA-CoA, structural alignment between DmdC and acyl-CoA dehydrogenase ACDH-11 (ACDH-11) in complex with C11-CoA from *Caenorhabditis elegans* (PDB code: 4Y9J) (Ma *et al.*, 2015) was performed to study the catalytic mechanism of DmdC (Fig. 6B). The active centers and the FAD binding sites of DmdC and ACDH-11 are coincident. Since MMPA-CoA possesses similarities to C11-CoA, the binding site of MMPA-CoA in DmdC is likely very similar to that of C11-CoA in ACDH-11. Therefore, some residues surrounding the possible binding site of MMPA-CoA in DmdC were identified based on the location of C11-CoA, which are Met161, Lys223, His280, Lys281, Arg284, Phe287, Tyr434, Glu435 and Arg448 (Fig. 6C). Site-directed mutations of Met161, Lys223, Lys281, His280 and Tyr434 to Ala severely reduced the activity of DmdC, but did not affect its K_m value to MMPA-CoA (Tables 4 and 5), indicating that these residues are involved in MMPA-CoA catalysis. In contrast, mutations of Arg284, Phe287 and Arg448 to Ala significantly increased its K_m value to MMPA-CoA (Tables 4 and 5), suggesting that these three residues are involved in MMPA-CoA binding. Notably, mutation of Glu435 to Ala completely abolished the activity of DmdC (Table 4), suggesting its vital role in catalysis.

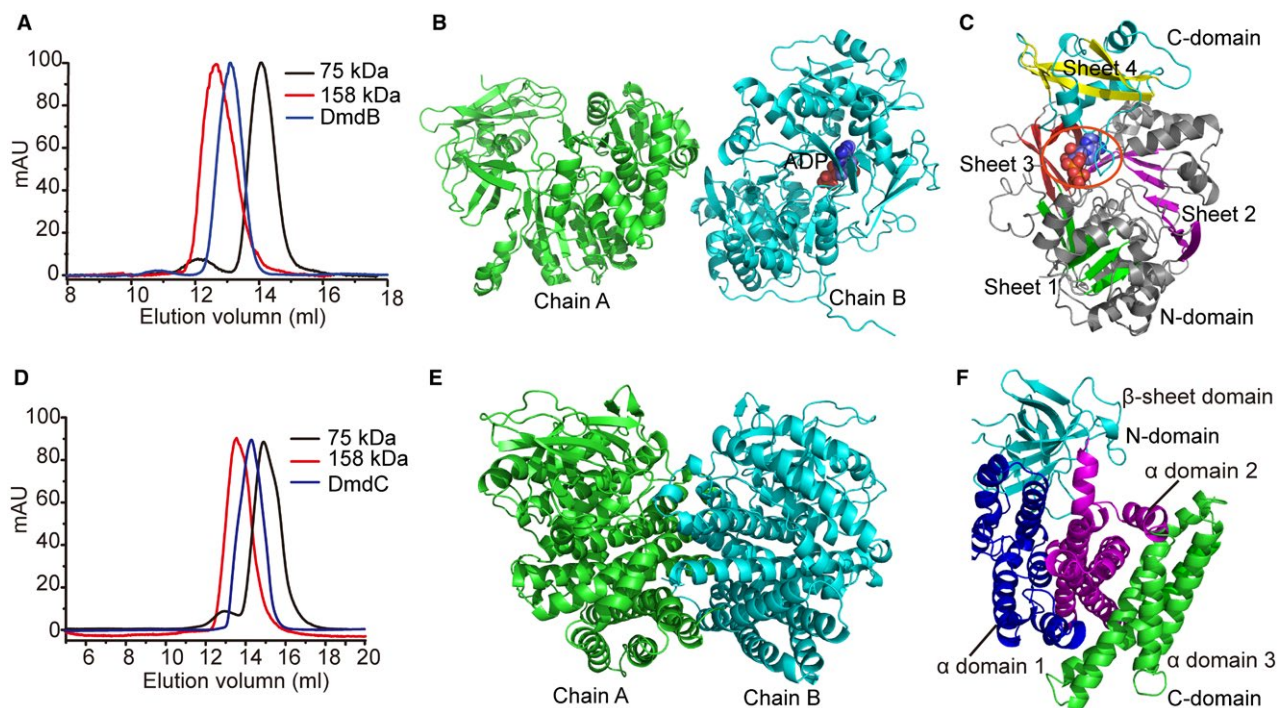


Fig. 4. Overall structures of DmdB from ITI-1157 and DmdC from ISM.

A. Association state analysis of DmdB in solution by gel filtration. Aldolase ($M_r = 75,000$ Da, GE Healthcare) and Conalbumin ($158,000$ Da, GE Healthcare) were used as markers. The molecular weight of DmdB monomer is $59,410$ Da. DmdB is a dimer in solution.
 B. Overall structure of DmdB. Chain A of DmdB is colored in green, and chain B in cyan. The ligand ADP is shown in the view of sphere.
 C. Overall structure of DmdB monomer. The N-domain contains three β -sheets (sheet 1, sheet 2 and sheet 3). The C-domain forms a five-stranded β -sheet (sheet 4) with three helices on its face. ADP is shown in the view of spheres. The active center is marked with a red circle.
 D. Association state analysis of DmdC in solution by gel filtration. Aldolase ($M_r = 75,000$ Da, GE Healthcare) and Conalbumin ($158,000$ Da, GE Healthcare) were used as markers. The molecular weight of DmdC is $64,210$ Da. DmdC is a dimer in solution.
 E. Overall structure of DmdC. The dimer is assembled through a large interface.
 F. Overall structure of DmdC monomer. It consists of four domains: an N-terminal α -helical domain (α -domain 1, colored in blue), a 10-stranded β sheet domain (colored in cyan), a central α -helical domain (α -domain 2, colored in purple) and a C-terminal α -helical domain (α -domain 3, colored in green). [Colour figure can be viewed at wileyonlinelibrary.com]

Structural alignment between DmdC and ACDH-11 suggests that the fatty acyl portion of C11-CoA is sandwiched between the isoalloxazine ring of FAD and residues of DmdC (Fig. 6D). Based on previous studies on acyl-CoA dehydrogenase family, the highly conserved Glu435 in the active center of DmdC is likely to be the catalytic residue (Fig. S5) (Kim *et al.*, 1993; Thorpe and Kim, 1995; Battaile *et al.*, 2002; Li and Nair, 2015). Glu435 is located parallel to the isoalloxazine ring of FAD with a distance of $6\text{--}7$ Å between them. The carboxyl oxygen of Glu435 faces the isoalloxazine ring, which is beneficial for the binding of MMPA-CoA between them to initiate the catalytic reaction (Ghisla and Thorpe, 2004; Bonito *et al.*, 2016). Moreover, the N5 of the isoalloxazine ring likely forms a hydrogen bond with Ser197, which enhances the electron deficient character of N5.

Based on our structural and mutational analyses and previous studies on acyl-CoA dehydrogenases (Massey and Ghisla, 1974; Pohl *et al.*, 1986; Kim *et al.*, 1993; Thorpe and Kim, 1995; Tamaoki *et al.*, 1999; Gulick *et al.*, 2004), we proposed the catalytic mechanism of DmdC for

MMPA-CoA redox reaction (Fig. 7C). In the active center of DmdC, FAD is stabilized by residues Met161, Thr170, Phe195, Ser197 and Tyr434, and the fatty acyl portion of MMPA-CoA is sandwiched between Glu435 and FAD (Fig. 6D). The negatively charged carboxyl group of Glu435 serves as the nucleophilic base to attack the C_α hydrogen of MMPA-CoA, and the abstraction of the C_α proton leads to the formation of a C_α carbanion. The carbanion attacks C_β , which weakens the C_β -H bond of MMPA-CoA. The electron deficient of N5 of the *p*-quinoid FAD is enhanced by the interaction with Ser197, and the C_β hydrogen, as a hydride ion, is directly transferred to the N5 position, leading to the formation of $C_\alpha=C_\beta$ of MTA-CoA (Fig. 7C). After FAD picking up the hydride, the carbonyl oxygen adjacent to the N1 becomes negatively charged (Fig. 7C). Consequently, MMPA-CoA is dehydrogenated to MTA-CoA, which is then released from the active center of DmdC.

To analyze how widespread this DmdC catalytic mechanism is in bacteria, we performed sequence alignment of bacterial DmdCs. The result showed that residue Glu435 and most of the residues involved in the binding of

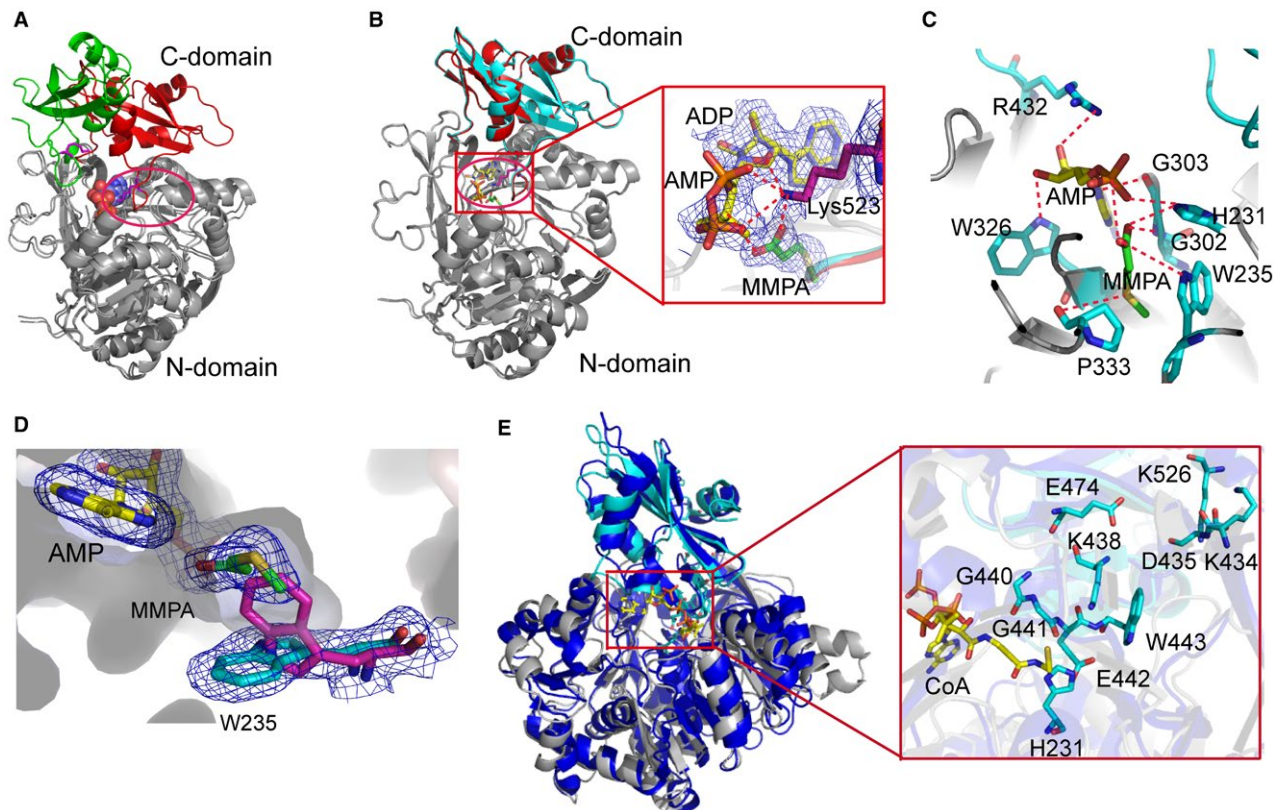


Fig. 5. Analyses of the DmdB structure and important residues in the active center.

A. Cartoon view of the structural alignment between two chains of DmdB/ADP complex. The C-domain of chain A is colored in green and that of chain B is colored in red. The conserved residue Lys523 in the two chains are shown in purple in the view of sticks. Ligand ADP is shown in blue in the view of sphere. The active center is marked with a red circle.

B. Cartoon view of the structural alignment between chain B of DmdB/ADP complex and that of Lys523Ala/AMP/MMPA complex. The C-domain of DmdB/ADP complex and that of Lys523Ala/AMP/MMPA complex are shown in red and cyan respectively. The residue Lys523 of DmdB/ADP complex is colored in purple. Ligands ADP, AMP and MMPA are colored in blue, yellow and green, respectively, in the view of sticks. Interactions of Lys523 with ADP, AMP and MMPA are shown in red dotted lines. The active center is marked with a red circle.

C. Important residues in the active center. Residues are shown in cyan sticks. AMP and MMPA are shown in yellow and green sticks respectively. Red dotted lines show the possible coordination bonds between the residues and the ligands AMP and MMPA.

D. Electrostatic surface view of the fatty-acid binding tunnel. Residue Trp235 in the absence of MMPA is shown in cyan sticks, and Trp235 in the presence of MMPA is shown in green sticks. MMPA is shown in purple sticks. Their densities are contoured in blue. The fatty-acid binding tunnel is shown in electrostatic surface view.

E. Cartoon view of the structural alignment between DmdB and 4-coumarate:CoA ligase (PDB code: 5BSR). The CoA molecule in 4-coumarate:CoA ligase is shown in yellow sticks. Important residues near the CoA molecule are shown in cyan sticks. The conformation of DmdB is a simulation result based on 4-coumarate:CoA ligase. [Colour figure can be viewed at wileyonlinelibrary.com]

MMPA-CoA and FAD are highly conserved in DmdCs from marine bacteria (once again including many roseobacters and the model SAR11 *P. ubique*) and nonmarine bacteria (Fig. S5), indicating that the proposed catalytic cycle of DmdC to oxidize MMPA-CoA is universally adopted by most of bacterial DmdCs.

The kinetic regulation of DMSP catabolism in DMSP-catabolizing Roseobacters

DMSP is catabolized by bacteria through the cleavage pathway and the demethylation pathway. The demethylation pathway in marine bacteria is reported to be responsible for the majority of environmental DMSP

catabolism (Kiene *et al.*, 1999; Reisch *et al.*, 2011a). We have demonstrated that the *dmd* genes are subject to transcription regulation, being transcribed at higher levels when grown in the presence of DMSP (Fig. 2), and this phenomenon are also found in the *ddd* genes from ITI-1157 and ISM (Fig. S6) (Wang *et al.*, 2015). Wang *et al.* (2017) proposed that the catabolism of DMSP and acrylate, the co-product of the DMSP cleavage pathway with DMS, in roseobacters is subject to kinetic regulation, which is governed by the K_m values of the sequential enzymatic steps in the DMSP catabolic pathway. To investigate whether a similar phenomenon exists in the DMSP demethylation pathway in Roseobacters, the K_m values of the enzymes involved in the demeth-

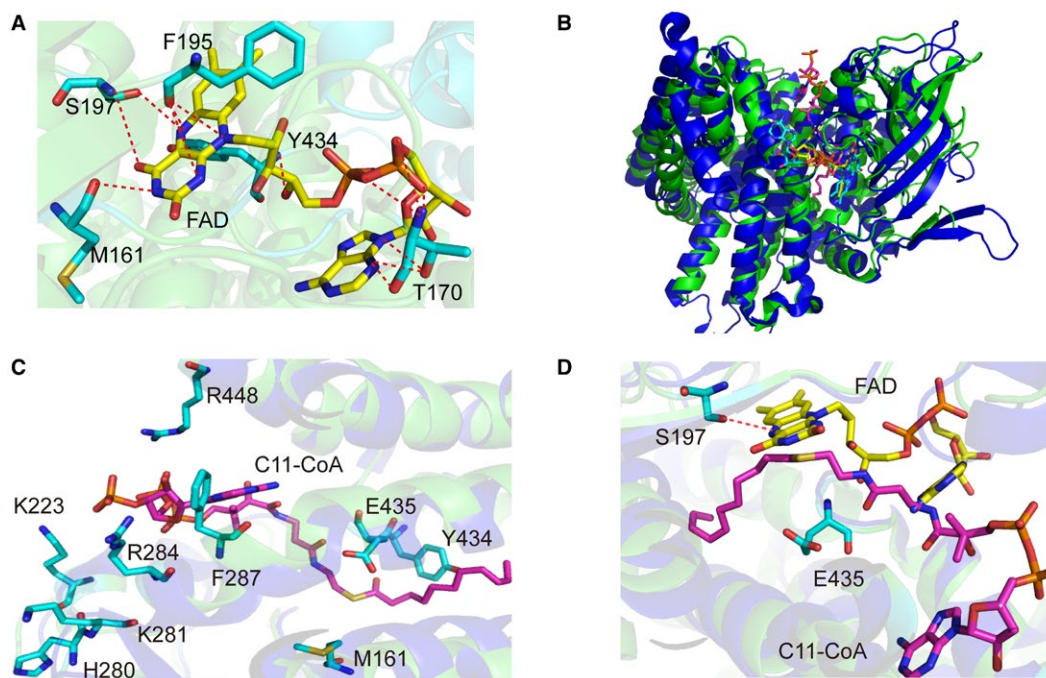


Fig. 6. Analyses of the DmdC structure and important residues in the active center.

A. Important residues in the DmdC active site and the possible coordination bonds between FAD and the residues. Residues are shown in cyan sticks. FAD is shown in yellow sticks.

B. Structural alignment between DmdC and ACDH-11 in complex with C11-CoA (PDB code: 4Y9J). The FAD and C11-CoA molecules in ACDH-11 are shown in cyan and purple sticks respectively. The FAD molecule in DmdC is shown in yellow sticks.

C. Important residues of DmdC in the possible binding site of MMPA-CoA deduced on structural alignment between DmdC and ACDH-11 (PDB code: 4Y9J). DmdC is shown in green cartoon, and ACDH-11 in blue cartoon. Residues are shown in cyan sticks. The C11-CoA molecule in ACDH-11 is shown in purple sticks.

D. The DmdC active site based on structural alignment with ACDH-11 (PDB code: 4Y9J). DmdC is shown in green cartoon, and ACDH-11 in blue cartoon. The FAD molecule in DmdC is shown in yellow sticks, and the C11-CoA molecule in ACDH-11 in purple sticks. Residues of DmdC are shown in cyan sticks. The fatty acyl portion of C11-CoA is sandwiched between Glu435 and FAD in the active center. [Colour figure can be viewed at wileyonlinelibrary.com]

Table 4. Enzymatic activities of the mutants of DmdC.^a

Enzyme	Relative activity (%)
Wild type	100
Met161Ala	37.5 ± 1.0
Thr170Ala	8.8 ± 2.3
Phe195Ala	0.4 ± 0.06
Ser197Ala	3.6 ± 0.3
Lys223Ala	9.4 ± 0.7
His280Ala	18.2 ± 0.5
Lys281Ala	54.5 ± 1.4
Arg284Ala	97.2 ± 2.7
Phe287Ala	76.3 ± 3.3
Tyr434Ala	51.2 ± 1.3
Glu435Ala	0.0 ^b
Arg448Ala	44.9 ± 2.0

^aRelative activity values expressed as a percentage of the specific activity of the wild type DmdC (100%). The standard errors are from three independent experiments. Specific activity in unit mg^{-1} of protein (\pm SE) defined as 100% was 7.9 ± 0.3 ($\mu\text{mol min}^{-1} \text{mg}^{-1}$).

^b<0.1%.

Table 5. K_m values of wild type DmdC and its mutants to different substrates.

Enzyme	K_m
To MMPA-CoA (mM)	
Wild type	1.4 ± 0.2
Met161Ala	6.3 ± 0.9
Lys223Ala	2.0 ± 0.2
His280Ala	2.0 ± 0.4
Lys281Ala	8.0 ± 1.3
Arg284Ala	12.4 ± 1.0
Phe287Ala	14.3 ± 1.3
Tyr434Ala	1.6 ± 0.2
Arg448Ala	>100
To FAD (μM)	
Wild type	6.3 ± 0.5
Met161Ala	9.2 ± 3.0
Thr170Ala	112.5 ± 4.5
Ser197Ala	64.8 ± 4.0
Tyr434Ala	29.9 ± 1.5

^aThe K_m values were determined by nonlinear analysis based on the initial rates of the reactions performed at pH 9.0 and 40°C. The standard errors are from three independent experiments.

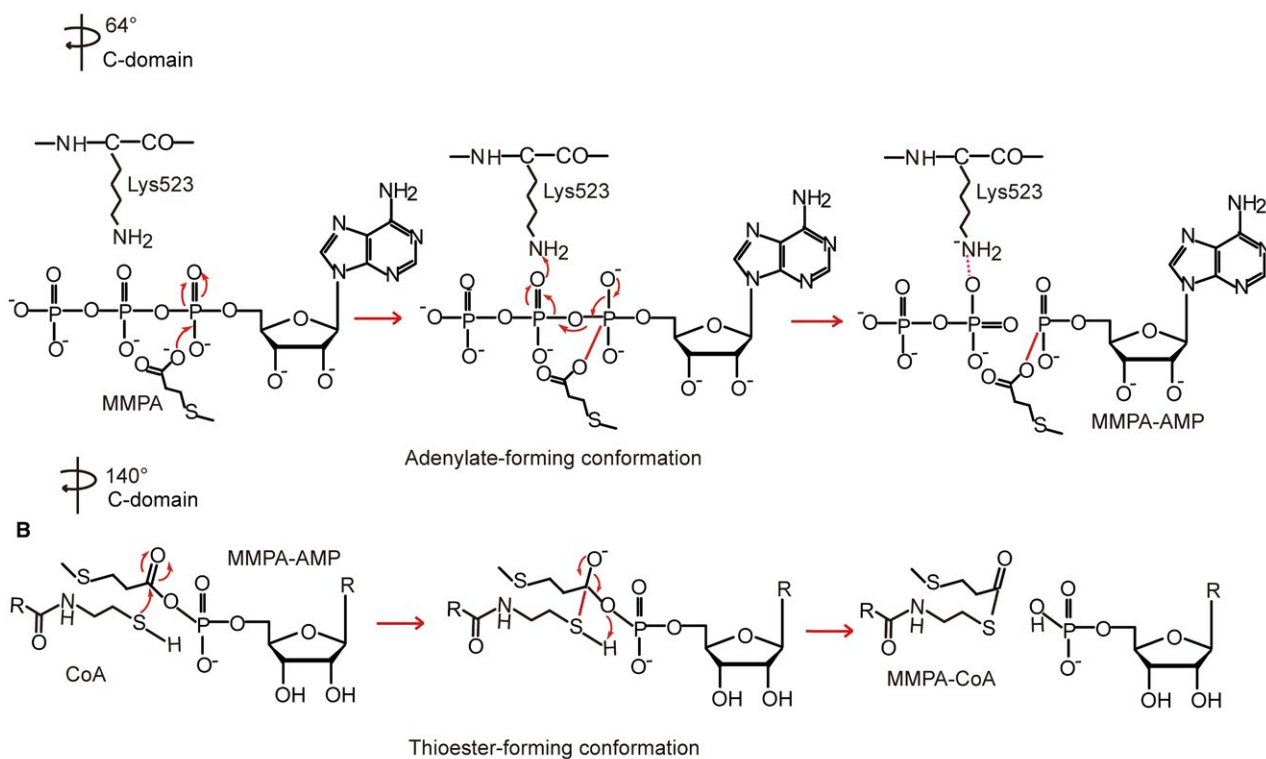
A Open conformation of DmdB

Fig. 7. A proposed catalytic mechanism for MMPA metabolism via DmdB and DmdC in Roseobacters.

A. The first half reaction of DmdB. Before the catalytic reaction, DmdB is in the open conformation. After a 64° rotation of the C-domain, DmdB turns into the adenylate-forming conformation, in which MMPA is ligated with AMP to form MMPA-AMP.

B. The second half reaction of DmdB. After a 140° rotation of the C-domain, DmdB turns into the thioester-forming conformation, in which AMP is released from MMPA-AMP and MMPA-CoA is formed.

C. The reaction of DmdC. MMPA-CoA is dehydrogenated by DmdC to form MTA-CoA. FAD is the cofactor to accept an electron. Residue Glu435 abstracts a proton from C_α of MMPA-CoA. The C_β hydrogen as a hydride is transferred to the N5 of FAD. [Colour figure can be viewed at wileyonlinelibrary.com]

ylation pathway from Roseobacters were investigated (Table 6). The K_m values of DmdAs from three Roseobacter strains are in the range from 4.10 mM to 35.66 mM (Reisch *et al.*, 2008), and that of a SAR11 strain is also in this range (13.2 mM) (Reisch *et al.*, 2008), which are at the same level as those of intracellular DMSP lyases in the cleavage pathway (Kirkwood

et al., 2010; Li *et al.*, 2014; Wang *et al.*, 2015). Therefore, the enzymes involved in the first step of DMSP catabolism in both the demethylation pathway and the cleavage pathway all have high K_m values at millimolar level, indicating that they all have a generally low affinity to DMSP (Wang *et al.*, 2017). The low affinities of DmdAs and intracellular DMSP lyases to DMSP are likely

Table 6. K_m values of DmdAs, DmdBs, DmdCs and DmdD.

Organism	Protein	Substrates	Products	Apparent K_m (mM)	Reference
<i>P. ubique</i> HTCC1062	DmdA	DMSP ^a , THF	MMPA, Methyl-THF	13.2 ± 2.0	Reisch <i>et al.</i> (2008)
<i>R. pomeroyi</i> DSS-3	DmdA	DMSP ^a , THF	MMPA, Methyl-THF	5.4 ± 2.3	Reisch <i>et al.</i> (2008)
<i>R. lacuscaerulensis</i> ITI-1157	DmdA	DMSP ^a , THF	MMPA, Methyl-THF	4.1 ± 0.4	This study
<i>R. nubinhibens</i> ISM	DmdA	DMSP ^a , THF	MMPA, Methyl-THF	35.7 ± 2.7	This study
<i>R. pomeroyi</i> DSS-3	DmdB	MMPA ^a , CoA, ATP	MMPA-CoA, AMP	1.7 ± 0.1	This study
<i>R. lacuscaerulensis</i> ITI-1157	DmdB	MMPA ^a , CoA, ATP	MMPA-CoA, AMP	0.3 ± 0.01	This study
<i>D. shibae</i> DFL 12	DmdB	MMPA ^a , CoA, ATP	MMPA-CoA, AMP	0.4 ± 0.05	This study
<i>S. stellata</i> E37	DmdB	MMPA ^a , CoA, ATP	MMPA-CoA, AMP	0.4 ± 0.03	This study
<i>R. pomeroyi</i> DSS-3	DmdC	MMPA-CoA ^a , FAD	MTA-CoA, FADH ₂	0.2 ± 0.01	This study
<i>R. lacuscaerulensis</i> ITI-1157	DmdC	MMPA-CoA ^a , FAD	MTA-CoA, FADH ₂	3.0 ± 0.5	This study
<i>R. nubinhibens</i> ISM	DmdC	MMPA-CoA ^a , FAD	MTA-CoA, FADH ₂	2.2 ± 0.4	This study
<i>D. shibae</i> DFL 12	DmdC	MMPA-CoA ^a , FAD	MTA-CoA, FADH ₂	2.7 ± 0.3	This study
<i>S. tellata</i> E37	DmdC	MMPA-CoA ^a , FAD	MTA-CoA, FADH ₂	1.5 ± 0.3	This study
<i>R. pomeroyi</i> DSS-3	DmdD	MTA-CoA ^a , H ₂ O	Acetaldehyde, MeSH, CoA, CO ₂	0.008	Tan <i>et al.</i> (2013)

Note: The K_m values analyzed in this study were determined by nonlinear analysis based on the initial rates of the reactions performed at the physiological conditions for each enzyme.

^aThe substrate for the K_m to be measured.

essential for bacteria to maintain a high intracellular DMSP concentration for its physiological functions, for example, osmoregulation and oxidative stress amelioration (Curson *et al.*, 2011; Reisch *et al.*, 2011a). Just like the K_m value of PrpE to acrylate in the cleavage pathway (Horswill and Escalante-Semerena, 2002; Wang *et al.*, 2017), the K_m values of DmdB and DmdC in the demethylation pathway are in millimolar levels, but, importantly, lower than that of DmdA, indicating that the affinities of DmdB and DmdC to their substrates are higher than that of DmdA. In contrast to the high substrate specificity of DmdA for DMSP, DmdB and DmdC are recruited from the pathways of methionine degradation and β -fatty acid oxidation (Reisch *et al.*, 2011a; 2011b). Comparison of the substrate specificities of DmdB/DmdC with their homologs in the same family indicated that most enzymes in the acyl-CoA ligase family and acyl-CoA dehydrogenase family have multiple substrate specificities (Table S1 and S2). DmdB is shown to have a higher affinity to MMPA than to acrylate, propionate or isobutyrate (Table S1) (Bullock *et al.*, 2014), implying the evolution of DmdB from other pathways to the demethylation pathway for DMSP catabolism. DmdC from *R. pomeroyi* DSS-3 has been reported to have lower K_m s to butyryl-CoA, valeryl-CoA and caproyl-CoA than to MMPA-CoA (Table S2) (Bullock *et al.*, 2017), indicating that MMPA-CoA might not be the optimal substrate of DmdC of *R. pomeroyi* DSS-3. Due to MTA-CoA were not commercially available and

difficult to prepare, we could not obtain the K_m value of AcuH to MTA-CoA, which has not been reported yet. However, DmdD has been reported to have a very low K_m value of 8 μ M (Table 6) and a high catalytic efficiency of 5400 $\text{mM}^{-1}\text{s}^{-1}$ (Tan *et al.*, 2013). Thus, DmdD has the highest affinity for its substrate of all the DMSP demethylation pathway enzymes and ensures the rapid, efficient and complete catabolism of DMSP through this pathway. A similar phenomenon is proposed in the acrylate catabolic pathway for the AcuL enzyme, which have quite low K_m values (1.1–2.8 μ M) and very high affinities to the toxic substrate acrylyl-CoA (Asao and Alber, 2013; Wang *et al.*, 2017). In addition, the very high affinity and catalytic efficiency of DmdD to MTA-CoA (Tan *et al.*, 2013) may imply that MTA-CoA may be a toxic compound if allowed to accumulate in DMSP-catabolizing Roseobacters. Indeed, the $C_{\alpha}=C_{\beta}$ and the carbonyl group of MTA-CoA (Fig. S7) forms a stable conjugated system that is a Michael acceptor, which makes MTA-CoA readily react with the thiol group of proteins by 1,4-addition, resulting in the alkylation proteins (Little *et al.*, 2004; Tanaka *et al.*, 1996). Just like methacrylyl-CoA and acryloyl-CoA, which both have the same Michael acceptor (Fig. S7) and are reported to be cytotoxic (Singh *et al.*, 1972; Dearfield *et al.*, 1991; Ishigure *et al.*, 2001; Herrmann *et al.*, 2010; Haack *et al.*, 2015), MTA-CoA is also potentially cytotoxic.

Based on the above analysis, it can be proposed that DMSP-catabolizing Roseobacters kinetically regulate

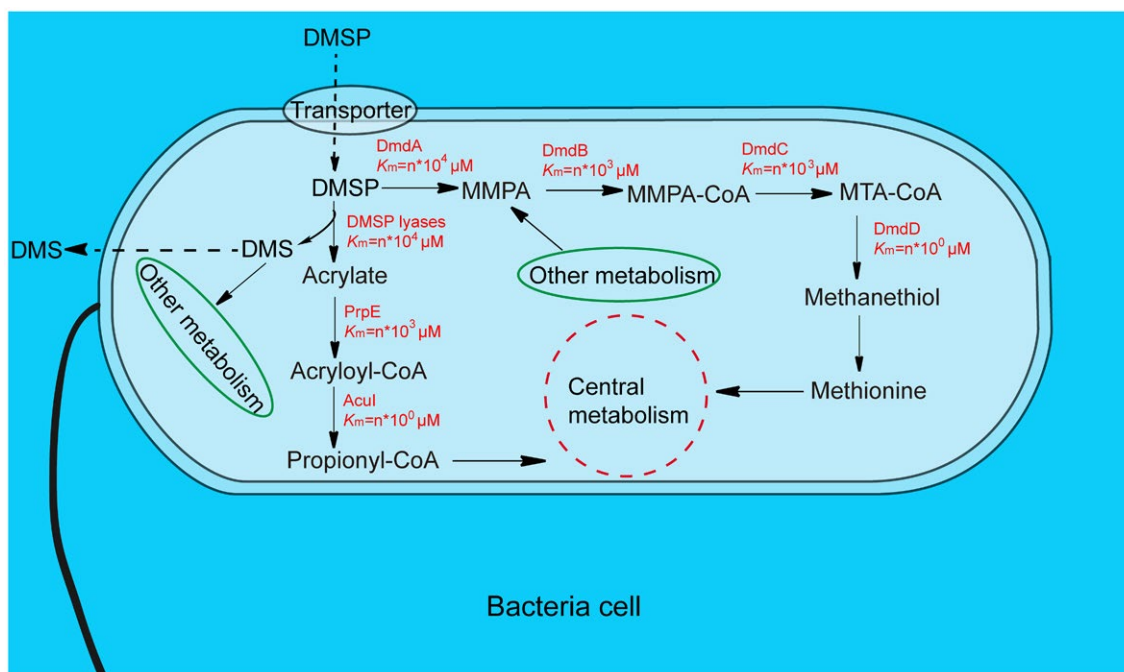


Fig. 8. The kinetically regulated DMSP catabolism pathways in DMSP-catabolizing Roseobacters. Through transport systems, environmental DMSP is concentrated to mM intracellular levels. DMSP is catabolized by two pathways, the cleavage pathway and the demethylation pathway, which kinetically regulate the catabolism of DMSP. The final products of these two pathways will finally enter the central metabolism. The K_m values of the enzymes are marked in red. [Colour figure can be viewed at wileyonlinelibrary.com]

the catabolism of DMSP. Firstly, the lower affinities of DmdA and DMS lyases enable the accumulation of DMSP to act its physiological functions. Secondly, the relatively increasing substrate affinities of DmdB, DmdC and PrpE are benefit for energy flow and substance transformation in the pathways. Lastly, the highest affinities of DmdD and Acul ensure the rapid catabolism of their harmful or toxic substrates and the completion of DMSP catabolism in bacterial cell for central metabolism (Fig. 8).

Conclusion

DMSP demethylation is the major environmental route for DMSP catabolism and is catabolized by four enzymes in Roseobacters, but the molecular mechanisms for the two central enzymes, DmdB and DmdC, were undetermined. DmdB and DmdC successively catabolise MMPA, the product of the DMSP demethylase DmdA, to generate MTA-CoA. Here, we demonstrate that the predicted DMSP demethylation genes in two model Roseobacter strains, IT-1157 and ISM, are functional. Based on structural and mutational analyses of DmdB and DmdC, we propose the catalytic mechanisms. DmdB undergoes two conformational changes to catalyze the ligation of MMPA and CoA, and DmdC catalyzes the dehydrogenation of

MMPA-CoA to generate MTA-CoA with Glu435 as the catalytic residue. Key residues identified to be involved in DmdB and DmdC catalysis are conserved in all the DmdB and DmdC sequences from marine bacteria (Figs. S4 and S5), and thus the proposed mechanisms may have universal significance among bacteria containing them, for example, in SAR11 and Roseobacter bacteria. Moreover, based on an investigation of the K_m values of all the enzymes involved in the demethylation, a kinetical regulation mechanism of DMSP demethylation in DMSP-catabolizing Roseobacters is revealed. Our results provide molecular insights into the metabolism of MMPA in DMSP-catabolizing Roseobacters and a better understanding of DMSP-involved marine carbon and sulfur cycling.

Experimental procedures

Bacterial strains and growth conditions

Strains ITI_1157 and ISM were purchased from the Leibniz Institute DSMZ-German Collection of Microorganism and were cultured in 514 medium at 40°C and 30°C, respectively, for two days according to the provided protocol (<http://www.dsmz.de/>). *E. coli* strains DH5 α and BL21 (DE3) were grown in Lysogeny Broth (LB) medium at 37°C.

Gene cloning, site-directed mutation, protein expression and purification

Genes were cloned from the genomes of ITI_1157 and ISM by PCR using *FastPfu* DNA polymerase (TransGen Biotech, China). PCR primers were all designed with *NdeI* and *HindIII* restriction sites, except that PCR primers of DmdB from ISM were designed with *EcoRI* and *HindIII* restriction sites. The amplified genes were recombined to the vector pET-22b (Novagen, Germany), and the recombinant plasmids were overexpressed in *E. coli* BL21 (DE3) cells. Site-directed mutations of DmdB and DmdC were performed with the QuikChange[®] mutagenesis kit II (Agilent, America). The recombinant *E. coli* strains were cultured at 37°C in LB medium to an OD₆₀₀ of 0.8–1.0 and then induced at 20°C for 16 h with 0.5 mM of isopropyl β-D-1-thiogalactopyranoside (IPTG). After induction, cells in the culture were collected by centrifugation, suspended in the buffer (50 mM of Tris-HCl, 100 mM of NaCl, 0.5% of glycerol, pH 8.0), and fractured by pressure crusher. Recombinant and mutant proteins were purified first by affinity chromatography on a His-Tag Ni-affinity column (GE Healthcare, America) equilibrated with 50 mM of Tris-HCl, pH 8.0, 100 mM of NaCl, 0.5% of glycerol, and then fractionated by anion exchange chromatography on a Source 15Q column eluted with 0–1M of NaCl in 50 mM of Tris-HCl, pH 8.0 at a flow rate of 3 ml/min and gel filtration on a Superdex G200 column (GE Healthcare, America) eluted with 10 mM of Tris-HCl, pH 8.0, 100 mM of NaCl at a flow rate of 0.5 ml/min.

Enzymatic assays

The enzymatic activity of DmdA toward DMSP (TCI, Japan) was measured by determining the production of MMPA by HPLC on a SunFire C₁₈ column (Waters, America) with a linear gradient of 2–20% acetonitrile in 50 mM ammonium acetate (pH 5.5) over 24 min at 210 nm. Enzyme assays were performed as described by Reisch *et al.* (2008). The control group had the same reaction system with the experimental group except that DmdA was not added.

The enzymatic activity of DmdB toward MMPA (Shanghai Yuanye, China) was measured by determining the production of AMP by HPLC on a SunFire C₁₈ column (Waters, America) with a linear gradient of 2–20% acetonitrile in 50 mM ammonium acetate (pH 5.5) over 24 min at 260 nm. Enzyme assay mixture contained 0.5 mM of MMPA, 2 mM of CoA, 0.5 mM of ATP, 5 mM of MgCl₂, 100 mM of Tris/HCl (pH 8.0) and 0.5 μM of purified DmdB. The reaction was performed at the optimal temperature (40°C) and pH (8.0) for 10 min, and was stopped by adding 10% hydrochloric acid. The control group had the same reaction system except that DmdB was not added. The K_m values of DmdB and its mutants were determined by non-linear analysis based on the initial rates, and all the measurements were performed at the optimal pH and temperature.

The enzymatic activity of DmdC toward MMPA-CoA was measured by determining the production of MTA-CoA by HPLC on a SunFire C₁₈ column (Waters, America) with a linear gradient of 2–20% acetonitrile in 50 mM of ammonium acetate (pH 5.5) over 24 min at 260 nm. MMPA-CoA

was synthesized enzymatically as describe by Reisch *et al.* (2011b). The enzyme assay mixture contained 1mM of MMPA-CoA, 0.5 mM of FAD, 50 mM of Tris/HCl and 1 mM of purified DmdC. The reaction was performed at 40°C and pH 9.0 for 30 min, and was stopped by adding 10% of hydrochloric acid. The control assay had the same reaction system except that DmdC was not added. The K_m values of DmdC and its mutants were determined by non-linear analysis based on the initial rates, and all the measurements were performed at the optimal pH (9.0) and temperature (40°C).

The enzymatic activity of AcuH toward MTA-CoA was measured by determining the reduction of substrate MTA-CoA by HPLC. The enzyme assay mixture contained 1 mM of MMPA-CoA, 0.5 mM of FAD, 50 mM of Tris/HCl, 5 mM of purified DmdC and 2 mM of purified AcuH. MTA-CoA was produced by DmdC catalyzing MMPA-CoA. The reaction was performed at 37°C and pH 8.0 for 2 h, and was stopped by adding 10% of hydrochloric acid (Cao *et al.*, 2017). The control assay had the same reaction system except that DmdC was not added.

In these assays, 1 unit was defined as 1 μmol product formed min⁻¹, and specific activity was defined as 1 unit per mg of protein.

Crystallization, data collection, structure determination and refinement

Both DmdB from ITI_1157 and DmdC from ISM were crystallized at 20°C using the sitting drop vapor diffusion method. The protein solution (10 mg/ml) was mixed with the reservoir solution with 1:1 ratio. The wild type DmdB was mixed with ADP at a molar ratio of 1:10. The mutant Lys523Ala was mixed with AMP and MMPA at a molar ratio of 1:10:10. All of the mixtures were incubated at 0°C for 15 min. The crystals of DmdB complexes were obtained in a buffer containing 0.2 M of sodium formate, 0.1 M of Bis-Tris propane (pH 7.5) and 20% (w/v) PEG 3350. The crystals of wild type DmdC were obtained in a buffer containing 0.2 M of sodium nitrate, 0.1 M of Bis-Tris propane (pH 8.5) and 20% (w/v) PEG 3350. X-ray diffraction data were collected on BL17U1 beamline at the Shanghai Synchrotron Radiation Facility using detector ADSC Quantum 315r. The initial diffraction datasets were processed by HKL2000.

Phase problems were solved by molecular replacement method (EPMR) using the CCP4 program phaser. The refinement was done by Phenix and Coot alternately. All the structure figures were processed using the program PyMOL (<http://www.pymol.org/>).

Circular dichroism spectroscopy

Circular dichroism (CD) spectra for wild type DmdB and DmdC and their mutants were recorded at 25°C on a J-810 spectropolarimeter (Jasco, Japan). All the spectra of the proteins at a concentration of 10 μM in 10 mM of Tris-HCl (pH 8.0) and 100 mM of NaCl were collected from 250 to 200 nm at a scan speed of 200 nm min⁻¹ using a quartz cell of 0.1 cm path length.

Molecular docking simulation

Molecular docking simulation between FAD and DmdC was performed using Autodock software (Morris *et al.*, 2009). The structure of FAD molecule was downloaded from the PDB (code: 4Y9J) (Ma *et al.*, 2015). The docking searches were executed using the Lamarckian genetic algorithm with a maximum number of 25,000,000 energy evaluations and the default settings for all other options. A total of 20 solutions were recorded, and only the first ranked solution, which carries the lowest binding energy reported by AutoDock, was collected for further analysis.

Accession numbers

The structures of DmdB in complex with ADP, Lys523Ala in complex with AMP and MMPA and apo-DmdC were deposited in the Protein Data Bank under the accession codes 6IHK, 6IJB and 6IJC respectively.

Real-time qPCR analysis

The cells of ITI_1157 and ISM were cultured in 2216E medium (BD, America) at 40°C and 30°C respectively. When the experimental groups containing 2 mM DMSP and the control groups containing no DMSP grew to an OD₆₀₀ of 0.8, RNA was extracted using the RNeasy mini kit (Qiagen, America), and was subsequently reverse-transcribed to cDNA using Goldenstar™RT6 cDNA Synthesis Kit (TsingKe, China), and then qPCR was performed using a Light Cycler II 480 System (Roche, Switzerland) following the instructions of SYBR® Premix Ex Taq™ (TaKaRa, Japan) with the following cycling conditions: 95°C for 5 min, 45 cycles of 95°C for 10 s and 60°C for 30 s. The *recA* gene was used as the house keeping gene.

Acknowledgements

We thank the staffs from BL18U1&BL19U1 beamlines of National Facility for Protein Sciences Shanghai (NFPS) and Shanghai Synchrotron Radiation Facility, for assistance during data collection. This work was supported by the National Key Research and Development Program of China (2018YFC1406700), the National Science Foundation of China (31630012, 91851205, 41706152, 31728001 and 31800107), the Program of Shandong for Taishan Scholars (TS20090803), and AoShan Talents Cultivation Program Supported by Qingdao National Laboratory for Marine Science and Technology (2017ASTCP-OS14), the Natural Science Foundation of Jiangsu Province (BK20170397), the Natural Science Foundation of Shandong Province (ZR2017BC079) and in JDT's lab by the Natural Environment Research Council standard grants NE/P012671/1 and NE/N002385/1.

References

And, G.J. and Tong, L. (2004) Crystal structure of yeast acetyl-coenzyme A synthetase in complex with AMP†. *Biochemistry*, **43**, 1425–1431.

Archer, S.D., Widdicombe, C.E., Tarran, G.A., Rees, A.P. and Burkill, P.H. (2001) Production and turnover of particulate dimethylsulphoniopropionate during a coccolithophore bloom in the northern North Sea. *Aquatic Microbial Ecology*, **24**, 225–241.

Asao, M. and Alber, B.E. (2013) Acrylyl-coenzyme A reductase, an enzyme involved in the assimilation of 3-hydroxypropionate by *Rhodobacter sphaeroides*. *Journal of Bacteriology*, **195**, 4716–4725.

Battaile, K.P., Molincase, J., Paschke, R., Wang, M., Bennett, D., Vockley, J. *et al.* (2002) Crystal structure of rat short chain acyl-CoA dehydrogenase complexed with acetoacetyl-CoA: comparison with other acyl-CoA dehydrogenases. *Journal of Biological Chemistry*, **277**, 12200–12207.

Bonito, C.A., Leandro, P., Ventura, F.V. and Guedes, R.C. (2016) Insights into medium-chain acyl-CoA dehydrogenase structure by molecular dynamics simulations. *Chemical Biology & Drug Design*, **88**, 281–292.

Bullock, H.A., Reisch, C.R., Burns, A.S., Moran, M.A. and Whitman, W.B. (2014) Regulatory and functional diversity of methylmercaptopropionate coenzyme A ligases from the dimethylsulfonylpropionate demethylation pathway in *Ruegeria pomeroyi* DSS-3 and other Proteobacteria. *Journal of Bacteriology*, **196**, 1275–1285.

Bullock, H.A., Luo, H. and Whitman, W.B. (2017) Evolution of dimethylsulfonylpropionate metabolism in marine phytoplankton and bacteria. *Frontiers in Microbiology*, **8**, 637.

Cao, H.Y., Wang, P., Xu, F., Li, P.Y., Xie, B.B., Qin, Q-L. *et al.* (2017) Molecular insight into the acryloyl-CoA hydration by AcuH for acrylate detoxification in dimethylsulfonylpropionate-catabolizing bacteria. *Frontiers in Microbiology*, **8**, 2034.

Chowdhury, N.P., Mowafy, A.M., Demmer, J.K., Upadhyay, V., Koelzer, S., Jayamani, E. *et al.* (2014) Studies on the mechanism of electron bifurcation catalyzed by electron transferring flavoprotein (Etf) and butyryl-CoA dehydrogenase (Bcd) of acid aminococcus fermentans. *Journal of Biological Chemistry*, **289**, 5145–5157.

Conti, E., Franks, N.P. and Brick, P. (1996) Crystal structure of firefly luciferase throws light on a superfamily of adenylate-forming enzymes. *Structure*, **4**, 287–298.

Conti, E., Stachelhaus, T., Marahiel, M.A. and Brick, P. (1997) Structural basis for the activation of phenylalanine in the non-ribosomal biosynthesis of gramicidin S. *Embo Journal*, **16**, 4174–4183.

Curson, A.R., Liu, J., Bermejo, M.A., Green, R.T., Chan, Y., Carrión, O. *et al.* (2017) Dimethylsulfonylpropionate biosynthesis in marine bacteria and identification of the key gene in this process. *Nature Microbiology*, **2**, 17009.

Curson, A.R., Todd, J.D., Sullivan, M.J. and Johnston, A.W. (2011) Catabolism of dimethylsulphonylpropionate: microorganisms, enzymes and genes. *Nature Reviews Microbiology*, **9**, 849–859.

Dearfield, K.L., Harrington-Brock, K., Doerr, C.L., Rabinowitz, J.R. and Moore, M.M. (1991) Genotoxicity in mouse lymphoma cells of chemicals capable of Michael addition. *Mutagenesis*, **6**, 519–525.

Ghisla, S., Thorpe, C. and Massey, V. (1984) Mechanistic studies with general acyl-CoA dehydrogenase and butyryl-CoA dehydrogenase: evidence for the transfer of the

- beta-hydrogen to the flavin N(5)-position as a hydride. *Biochemistry*, **23**, 3154–3161.
- Ghisla, S. and Thorpe, C. (2004) Acyl-CoA dehydrogenases. A mechanistic overview. *European Journal of Biochemistry*, **271**, 494–508.
- González, J.M., Covert, J.S., Whitman, W.B., Henriksen, J.R., Mayer, F., Scharf, B. *et al.* (2003) *Silicibacter pomeroyi* sp. nov. and *Roseovarius nubinhibens* sp. nov., dimethylsulfoniopropionate-demethylating bacteria from marine environments. *International Journal of Systematic & Evolutionary Microbiology*, **53**, 1261–1269.
- Gulick, A.M., Lu, X. and Dunawaymariano, D. (2004) Crystal structure of 4-chlorobenzoate:CoA ligase/synthetase in the unliganded and aryl substrate-bound states. *Biochemistry*, **43**, 8670.
- Gulick, A.M., Starai, V.J., Horswill, A.R., Homick, K.M. and Escalante-Semerena, J.C. (2003) The 1.75 Å crystal structure of acetyl-CoA synthetase bound to adenosine-5'-propylphosphate and coenzyme A. *Biochemistry*, **42**, 2866–2873.
- Haack, T.B., Jackson, C.B., Murayama, K., Kremer, L.S., Schaller, A., Kotzaeridou, U. *et al.* (2015) Deficiency of ECHS1 causes mitochondrial encephalopathy with cardiac involvement. *Annals of Clinical & Translational Neurology*, **2**, 492–509.
- Herrmann, G., Selmer, T., Jessen, H.J., Gokarn, R.R., Selifonova, O., Gort, S.J. *et al.* (2010) Two beta-allyl-CoA:ammonia lyases in *Clostridium propionicum*. *Febs Journal*, **272**, 813–821.
- Hilgenberg, W. (1985) ADP is a competitive inhibitor of ATP-dependent H⁺ transport in microsomal membranes from *Zea mays* L. coleoptiles. *Plant Physiology*, **77**, 881–885.
- Hisanaga, Y., Ago, H., Nakagawa, N., Hamada, K., Ida, K., Yamamoto, M. *et al.* (2004) Structural basis of the substrate-specific two-step catalysis of long chain fatty acyl-CoA synthetase dimer. *Journal of Biological Chemistry*, **279**, 31717–31726.
- Horswill, A.R. and Escalante-Semerena, J.C. (2002) Characterization of the propionyl-CoA synthetase (PrpE) enzyme of *Salmonella enterica*: residue Lys592 is required for propionyl-AMP synthesis. *Biochemistry*, **41**, 2379–2387.
- Howard, E.C., Henriksen, J.R., Buchan, A., Reisch, C.R., Bürgmann, H., Welsh, R. *et al.* (2006) Bacterial taxa that limit sulfur flux from the ocean. *Science*, **314**, 649–652.
- Ishigure, K., Shimomura, Y., Murakami, T., Kaneko, T., Takeda, S., Inoue, S. *et al.* (2001) Human liver disease decreases methacrylyl-CoA hydratase and β-hydroxyisobutyryl-CoA hydrolase activities in valine catabolism☆. *Clinica Chimica Acta*, **312**, 115–121.
- Kiene, R.P., Linn, L.J., González, J., Moran, M.A. and Bruton, J.A. (1999) Dimethylsulfoniopropionate and methanethiol are important precursors of methionine and protein-sulfur in marine bacterioplankton. *Applied & Environmental Microbiology*, **65**, 4549–4558.
- Kim, J.J., Wang, M. and Paschke, R. (1993) Crystal structures of medium-chain acyl-CoA dehydrogenase from pig liver mitochondria with and without substrate. *Proceedings of the National Academy of Sciences of the United States of America*, **90**, 7523–7527.
- Kirkwood, M., Todd, J.D., Rypien, K.L. and Johnston, A.W. (2010) The opportunistic coral pathogen *Aspergillus sydowii* contains dddP and makes dimethyl sulfide from dimethylsulfoniopropionate. *The International Society for Microbial Ecology Journal*, **4**, 147–150.
- Kochan, G., Pilka, E.S., Von, F.D., Oppermann, U. and Yue, W.W. (2009) Structural snapshots for the conformation-dependent catalysis by human medium-chain acyl-coenzyme A synthetase ACSM2A. *Journal of Molecular Biology*, **388**, 997–1008.
- Ksionzek, K.B., Lechtenfeld, O.J., McCallister, S.L., Schmitt-Kopplin, P., Geuer, J.K., Geibert, W. *et al.* (2016) Dissolved organic sulfur in the ocean: biogeochemistry of a petagram inventory. *Science*, **354**, 456–459.
- Li, C.Y., Wei, T.D., Zhang, S.H., Chen, X.L., Gao, X., Wang, P. *et al.* (2014) Molecular insight into bacterial cleavage of oceanic dimethylsulfoniopropionate into dimethyl sulfide. *Proceedings of the National Academy of Sciences of the United States of America*, **111**, 1026–1031.
- Li, Z. and Nair, S. (2015) Structural basis for specificity and flexibility in a plant 4-coumarate:CoA ligase. *Structure*, **23**, 2032–2042.
- Little, R.D., Masjedizadeh, M.R., Wallquist, O. and McLoughlin, J.I. (2004) *The Intramolecular Michael Reaction*. New York: John Wiley & Sons Inc.
- Ma, D.K., Li, Z., Lu, A.Y., Sun, F., Chen, S., Rothe, M. *et al.* (2015) Acyl-CoA dehydrogenase drives heat adaptation by sequestering fatty acids. *Cell*, **161**, 1152–1163.
- Massey, V. and Ghisla, S. (1974) Role of charge-transfer interactions in flavoprotein catalysis. *Annals of the New York Academy of Sciences*, **227**, 446–465.
- May, J.J., Kessler, N., Marahiel, M.A. and Stubbs, M.T. (2002) Crystal structure of DhbE, an archetype for aryl acid activating domains of modular nonribosomal peptide synthetases. *Proceedings of the National Academy of Sciences of the United States of America*, **99**, 12120–12125.
- Morris, G.M., Huey, R., Lindstrom, W., Sanner, M.F., Belew, R.K., Goodsell, D.S. *et al.* (2009) AutoDock4 and AutoDockTools4: Automated docking with selective receptor flexibility. *Journal of Computational Chemistry*, **30**, 2785–2791.
- Peterson, K.L., Sergienko, E.E., Wu, Y., Kumar, N.R., Strauss, A.W., Oleson, A.E. *et al.* (1995) Recombinant human liver medium-chain acyl-CoA dehydrogenase: purification, characterization, and the mechanism of interactions with functionally diverse C8-CoA molecules. *Biochemistry*, **34**, 14942–14953.
- Petursdottir, S.K. and Kristjansson, J.K. (1997) *Silicibacter lacuscaerulensis* gen. nov., sp. nov., a mesophilic moderately halophilic bacterium characteristic of the Blue Lagoon geothermal lake in Iceland. *Extremophiles Life Under Extreme Conditions*, **1**, 94–99.
- Pohl, B., Raichle, T. and Ghisla, S. (1986) Studies on the reaction mechanism of general acyl-CoA dehydrogenase. *European Journal of Biochemistry*, **160**, 109–115.
- Pratt, M.L. and Roche, T.E. (1979) Mechanism of pyruvate inhibition of kidney pyruvate dehydrogenase kinase and synergistic inhibition by pyruvate and ADP. *Journal of Biological Chemistry*, **254**, 7191–7196.
- Reger, A.S., Carney, J.M. and Gulick, A.M. (2007) Biochemical and crystallographic analysis of substrate binding and conformational changes in acetyl-CoA synthetase. *Biochemistry*, **46**, 6536–6546.

- Reisch, C.R., Ann, M.M. and Whitman, W.B. (2011a) Bacterial catabolism of dimethylsulfoniopropionate (DMSP). *Frontiers in Microbiology*, **2**, 172.
- Reisch, C.R., Moran, M.A. and Whitman, W.B. (2008) Dimethylsulfoniopropionate-dependent demethylase (DmdA) from *Pelagibacter ubique* and *Silicibacter pomeroyi*. *Journal of Bacteriology*, **190**, 8018–8024.
- Reisch, C.R., Stoudemayer, M.J., Varaljay, V.A., Amster, I.J., Moran, M.A. and Whitman, W.B. (2011b) Novel pathway for assimilation of dimethylsulphoniopropionate widespread in marine bacteria. *Nature*, **473**, 208–211.
- Roche, T.E. and Reed, L.J. (1974) Monovalent cation requirement for ADP inhibition of pyruvate dehydrogenase kinase. *Biochemical and Biophysical Research Communications*, **59**, 1341–1348.
- Schuller, D.J., Reisch, C.R., Moran, M.A., Whitman, W.B. and Lanzilotta, W.N. (2012) Structures of dimethylsulfoniopropionate-dependent demethylase from the marine organism *Pelagabacter ubique*. *Protein Science A Publication of the Protein Society*, **21**, 289–298.
- Singh, A.R., Lawrence, W.H. and Autian, J. (1972) Embryonic-fetal toxicity and teratogenic effects of a group of methacrylate esters in rats. *Journal of Dental Research*, **51**, 1632–1638.
- Tamaoki, H., Nishina, Y., Shiga, K. and Miura, R. (1999) Mechanism for the recognition and activation of substrate in medium-chain acyl-CoA dehydrogenase. *Journal of Biochemistry*, **125**, 285–296.
- Tan, D., Crabb, W.M., Whitman, W.B. and Tong, L. (2013) Crystal structure of DmdD, a crotonase superfamily enzyme that catalyzes the hydration and hydrolysis of methylthioacryloyl-CoA. *Plos One*, **8**, e63870.
- Tanaka, K., Inoue, T., Tezuka, Y. and Kikuchi, T. (1996) Michael-type addition of illudin S, a toxic substance from *Lampteromyces japonicus*, with cysteine and cysteine-containing peptides *in vitro*. *Chemical & Pharmaceutical Bulletin*, **27**, 273–279.
- Thorpe, C. and Kim, J.J. (1995) Structure and mechanism of action of the acyl-CoA dehydrogenases. *Faseb Journal Official Publication of the Federation of American Societies for Experimental Biology*, **9**, 718–725.
- Todd, J.D., Curson, A.R., Sullivan, M.J., Kirkwood, M. and Johnston, A.W.B. (2012) The *Ruegeria pomeroyi* acul gene has a role in DMSP catabolism and resembles yhdH of *E. coli* and other bacteria in conferring resistance to acrylate. *Plos One*, **7**, e35947.
- Visscher, P.T., Kiene, R.P. and Taylor, B.F. (1994) Demethylation and cleavage of dimethylsulfoniopropionate in marine intertidal sediments. *FEMS Microbiology Ecology*, **14**, 179–189.
- Wang, P., Chen, X.L., Li, C.Y., Gao, X., Zhu, D.Y., Xie, B.-B. *et al.* (2015) Structural and molecular basis for the novel catalytic mechanism and evolution of DddP, an abundant peptidase-like bacterial dimethylsulfoniopropionate lyase: a new enzyme from an old fold. *Molecular Microbiology*, **98**, 289–301.
- Wang, P., Cao, H.Y., Chen, X.L., Li, C.Y., Li, P.Y., Zhang, X.-Y. *et al.* (2017) Mechanistic insight into acrylate metabolism and detoxification in marine dimethylsulfoniopropionate-catabolizing bacteria. *Molecular Microbiology*, **105**, 674–688.

Supporting Information

Additional supporting information may be found online in the Supporting Information section at the end of the article